EBioMedicine 16 (2017) 224–237

Contents lists available at ScienceDirect

EBioMedicine

journal homepage: www.ebiomedicine.com

Research Paper

p53 Modulates the Fate of Cardiac Progenitor Cells Ex Vivo and in the Diabetic Heart In Vivo

Ramaswamy Kannappan [a,1], Alex Matsuda [a,b,1], João Ferreira-Martins [a], Eric Zhang [a], Giorgia Palano [a], Anna Czarna [a,b], Mauricio Castro Cabral-Da-Silva [a], Adriana Bastos-Carvalho [a], Fumihiro Sanada [a], Noriko Ide [a], Marcello Rota [a], Maria A. Blasco [c], Manuel Serrano [c], Piero Anversa [a,b], Annarosa Leri [a,b,*]

[a] Departments of Anesthesia and Medicine, and Division of Cardiovascular Medicine, Brigham and Women's Hospital, Harvard Medical School, Boston, MA 02115, USA
[b] Cardiocentro Ticino Foundation, Swiss Institute for Regenerative Medicine (SIRM), Via Tesserete 48, 6900 Lugano, Switzerland
[c] Spanish National Cancer Research Centre (CNIO), Madrid E-28029, Spain.

ARTICLE INFO

Article history:
Received 9 November 2016
Received in revised form 20 January 2017
Accepted 20 January 2017
Available online 31 January 2017

Keywords:
Stem cell engraftment
Diabetes
DNA repair
Stem cell fate

ABSTRACT

p53 is an important modulator of stem cell fate, but its role in cardiac progenitor cells (CPCs) is unknown. Here, we tested the effects of a single extra-copy of p53 on the function of CPCs in the presence of oxidative stress mediated by doxorubicin in vitro and type-1 diabetes in vivo. CPCs were obtained from super-p53 transgenic mice (p53-tg), in which the additional allele is regulated in a manner similar to the endogenous protein. Old CPCs with increased p53 dosage showed a superior ability to sustain oxidative stress, repair DNA damage and restore cell division. With doxorubicin, a larger fraction of CPCs carrying an extra-copy of the p53 allele recruited γH2A.X reestablishing DNA integrity. Enhanced p53 expression resulted in a superior tolerance to oxidative stress in vivo by providing CPCs with defense mechanisms necessary to survive in the milieu of the diabetic heart; they engrafted in regions of tissue injury and in three days acquired the cardiomyocyte phenotype. The biological advantage provided by the increased dosage of p53 in CPCs suggests that this genetic strategy may be translated to humans to increase cellular engraftment and growth, critical determinants of successful cell therapy for the failing heart.

1. Introduction

Myocardial aging in animals and humans is characterized by an increase in number of resident cardiac progenitor cells (CPCs) expressing the senescence-associated protein $p16^{INK4a}$, which prevents permanently the reentry of stem cells into the cell cycle (Beausejour and Campisi, 2006; Dimmeler and Leri, 2008; Sanada et al., 2014; Leri et al., 2015). This age-dependent effect results in a reduction of the pool of functionally-competent CPCs in the old heart (Torella et al., 2004). Alterations of coronary blood flow and defects in the structural determinants of tissue oxygenation in the aging myocardium (Hachamovitch et al., 1989) create hypoxic micro-domains where CPCs are maintained in a quiescent state (Sanada et al., 2014), impairing the activation of a compartment of progenitor cells with relatively intact replicative reserve.

The tumor suppressor p53 is a major regulator of DNA repair and cell division, cellular aging and apoptosis (Riley et al., 2008). Phosphorylation of the N-terminal of p53 promotes DNA repair, a process that is intimately linked to the progression of the cell cycle. DNA repair may be less effective in old CPCs, resulting in the accumulation of DNA lesions, a phenomenon that favors cellular senescence. The expression of p53 increases with aging and heart failure (Leri et al., 2003; Cheng et al., 2013) but its actual role in CPCs is unknown; p53 may trigger apoptosis of old cells and may induce DNA repair in cells with a younger phenotype (Matheu et al., 2007).

Whether this potential youth promoting effect of p53 is determined by a successful DNA damage response (DDR), mediated by transient reparable DNA lesions in the telomeric and non-telomeric regions of the genome, remains to be defined. A prolonged DDR signaling may result in the accumulation of non-reparable DNA foci and initiation of cell death (Fumagalli et al., 2012). Moreover, these intrinsic variables of CPCs have implications in the outcome of cell therapy for the damaged heart, where the unfavorable conditions of the recipient myocardium with high levels of oxidative stress affect the survival and growth of the delivered cells. These questions have been addressed in the present

Abbreviations: CPC, cardiac progenitor cell; DDR, DNA damage response; WT, wild type; LV, left ventricle; p53-tg, super-p53 transgenic mouse; Aogen, angiotensinogen; Ang II, angiotensin II; AT1R, Ang II type-1 receptor; PDT, population doubling time; ROS, reactive oxygen species; Doxo, doxorubicin.

* Corresponding author at: Cardiocentro Ticino Foundation, Swiss Institute for Regenerative Medicine (SIRM), Via Tesserete 48, 6900 Lugano, Switzerland.
E-mail address: annarosa.leri@cardiocentro.org (A. Leri).

[1] Joint first authors.

http://dx.doi.org/10.1016/j.ebiom.2017.01.028

study by evaluating CPC aging in mice with enhanced expression of p53 and then by assessing CPC engraftment in the diabetic heart that is characterized by an environment in which the generation of reactive oxygen and inflammation condition its evolution (Rota et al., 2006).

The super-p53 mouse (p53-tg) (Garcia-Cao et al., 2002), which is based on a C57BL/6J genetic background, carries a single extra gene-dose of p53. This single-copy transgene is regulated in a manner similar to its endogenous counterpart; p53 is not constitutively active, but undergoes post-translational modifications in response to stress stimuli, resulting in a moderately higher p53 activity (Garcia-Cao et al., 2006). The increased gene dosage of p53 triggers an amplified DDR in lymphocytes, splenocytes, embryonic fibroblasts, and epithelial cells of the skin and intestine (Garcia-Cao et al., 2002), but its impact on CPC aging and growth reserve has never been determined. Because of these characteristics, this animal model was considered relevant for understanding the role of p53 in CPC function with aging and oxidative stress.

2. Methods

2.1. Animals

All procedures were approved by the Institutional Animal Care and Use Committee of the Brigham and Women's Hospital. Animals received humane care in compliance with the "Guide for the Care and Use of Laboratory Animals" as described by the Institute of Laboratory Animal Research Resources, Commission on Life Sciences, National Research Council. Male and female wild-type (WT) and super p53 transgenic (p53-tg) mice in a C57BL/6 genetic background were studied (Garcia-Cao et al., 2002, 2006). WT and p53-tg at different ages were included in the protocols.

2.2. Ventricular Hemodynamics

Cardiac function was measured in young-adult, 3–6 months of age, and old, 24–31 months of age, WT and p53-tg mice. Left ventricular (LV) parameters (Leri et al., 2003; Torella et al., 2004; Rota et al., 2007; Sanada et al., 2014) were obtained in the closed chest preparation with a MPVS-400 system for small animals (Millar Instruments) equipped with a PVR-1045 catheter. Under sodium pentobarbital (50 mg/kg body weight, i.p.) anesthesia, the right carotid artery was exposed and the pressure transducer was inserted in the carotid artery and advanced into the LV cavity. Data were acquired and analyzed with Chart 5 (ADInstruments) software.

2.3. Myocyte Isolation

Under pentobarbital anesthesia, the heart was excised and LV myocytes were enzymatically dissociated (Torella et al., 2004; Rota et al., 2007; Signore et al., 2015). Briefly, the myocardium was perfused retrogradely through the aorta at 37 °C with a Ca^{2+}-free solution gassed with 85% O_2 and 15% N_2. After 5 min, 0.1 mM $CaCl_2$, 274 units/ml collagenase (type 2, Worthington Biochemical Corp.) and 0.57 units/ml protease (type XIV, Sigma) were added to the solution which contained (mM): NaCl 126, KCl 4.4, $MgCl_2$ 5, HEPES 20, Glucose 22, Taurine 20, Creatine 5, Na Pyruvate 5 and NaH_2PO_4 5 (pH 7.4, adjusted with NaOH). At completion of digestion, the LV was cut in small pieces and re-suspended in Ca^{2+} 0.1 mM solution. Myocytes were collected by differential centrifugation.

2.4. Ca^{2+} Transients and Sarcomere Shortening

Isolated LV myocytes were placed in a bath on the stage of an Axiovert Zeiss Microscope and IX71 Olympus inverted microscope for the measurements of contractility and Ca^{2+} transients. Experiments were conducted at room temperature. Cells were bathed continuously with a Tyrode solution containing (mM): NaCl 140, KCl 5.4, $MgCl_2$ 1, HEPES 5, Glucose 5.5 and $CaCl_2$ 1.0 (pH 7.4, adjusted with NaOH). Measurements were performed in field-stimulated cells by using IonOptix fluorescence and contractility systems (IonOptix, Milton, MA). Contractions were elicited by rectangular depolarizing pulses, 2 ms in duration, and twice-diastolic threshold in intensity, by platinum electrodes (Torella et al., 2004; Signore et al., 2015). Changes in mean sarcomere length were computed by determining the mean frequency of sarcomere spacing by fast Fourier transform and then frequency data were converted to length. Ca^{2+} transients were measured by epifluorescence after loading the myocytes with 10 μM Fluo-3 AM (Invitrogen). Excitation length was 480 nm with emission collected at 535 nm using a 40× oil objective. Fluo-3 signals were expressed as normalized fluorescence (F/F_0).

2.5. Immunohistochemistry

Following the acquisition of the hemodynamic parameters, the abdominal aorta was cannulated with a polyethylene catheter, PE-50, filled with a phosphate buffer, 0.2 M, pH 7.4, and heparin, 100 U/ml. In rapid succession, the heart was arrested in diastole by the injection of 0.15 ml of $CdCl_2$, 100 mM, through the aortic catheter, the thorax was opened, perfusion with phosphate buffer was started, and the vena cava was cut to allow drainage of blood and perfusate. After perfusion with phosphate buffer for 2 min, the coronary vasculature was perfused for 15 min with formalin. Subsequently, the heart was excised and embedded in paraffin (Leri et al., 2003; Torella et al., 2004; Rota et al., 2007; Sanada et al., 2014).

Formalin-fixed paraffin-embedded myocardial sections were labeled with goat polyclonal *anti*-*c*-kit (R&D: cat. no. AF1356), mouse monoclonal *anti*-α-sarcomeric actin (Sigma-Aldrich: clone 5C5, cat. no. A2172) to identify CPCs and cardiomyocytes, respectively. Nuclei were stained by DAPI. Cycling CPCs and cardiomyocytes were recognized by labeling with mouse monoclonal *anti*-Ki67 antibody (BD Biosciences: cat. no. 550609). Apoptotic and senescent cells were recognized by the TUNEL assay (Roche: cat. no. 11684795910) and $p16^{INK4a}$ localization (Cell Signaling: cat. no. 4824), respectively (Leri et al., 2003; Torella et al., 2004; Rota et al., 2007; Sanada et al., 2014). The number of *c*-kit-positive CPCs per unit area of myocardium in the atria and LV mid-region was determined as previously described (Torella et al., 2004; Sanada et al., 2014).

2.6. Western Blotting of Cardiomyocytes

Protein lysates of cardiomyocytes were obtained using RIPA buffer (Sigma) and protease inhibitors. Equivalents of 50 μg of proteins were separated on 10–12% SDS-PAGE, transferred onto PVDF membranes (Bio-Rad) and subjected to Western blotting with mouse monoclonal *anti*-Aogen (Swant: cat. no. 138), rabbit polyclonal *anti*-AT1R (Millipore: cat. no. 15552), rabbit polyclonal *anti*-Bax (Cell Signaling: cat. no. 7074) and rabbit polyclonal *anti*-Bcl2 (Cell Signaling: cat. no. D17C4) diluted 1:500–1000 in TBST or BSA overnight at 4 °C. HRP-conjugated *anti*-IgG were used as secondary antibodies. Proteins were detected by chemiluminescence (SuperSignal West Femto Maximum Sensitivity Substrate, Thermo Scientific: cat. no. 34095) and optical density was measured. Loading conditions were determined by Ponceau S (Sigma) staining of the membrane after transfer. Lung and kidney were used as positive controls for Aogen and AT1R, respectively. SVT2 and B16 melanoma cells were employed for the recognition of the bands corresponding to Bax and Bcl2, respectively (Leri et al., 1998; Torella et al., 2004; Goichberg et al., 2013).

2.7. CPC Isolation and Expansion

Following myocyte isolation, the small cardiac cell pool present in the supernatant was plated in Petri dishes and, 24 h later, *c*-kit positive cells were obtained by immunomagnetic sorting (Miltenyi Biotec.: cat.

no. 130-091-224) (Beltrami et al., 2003; D'Amario et al., 2011, 2014; Sanada et al., 2014). Subsequently, *c*-kit-positive cells were cultured in F12K medium supplemented with 10% fetal bovine serum. Immunomagnetic sorting for *c*-kit was repeated every three passages to select with this protocol the fraction of cells that retained *c*-kit expression. This approach was required because mouse *c*-kit-positive CPCs tend to lose this surface receptor with time in culture. When possible, immediately sorted cells were utilized; however, assays requiring large numbers of CPCs were conducted after cell expansion.

2.8. Population Doubling Time (PDT)

CPCs were plated at low density. The number of cells per unit area was determined at the time of seeding and 24 h later (D'Amario et al., 2011, 2014). PDT was computed by linear regression of $\log_2$ values of cell number.

2.9. Proliferation, Senescence and Apoptosis

These cellular parameters were measured in baseline conditions, following exposure to doxorubicin (Doxo; 0.5 μM) for 4 h, and 24, 48 and 72 h following removal of Doxo. Cells were fixed in 4% paraformaldehyde and the fraction of cycling cells was determined by immunolabeling for Ki67 (eBioscience: cat. no. 14-5698-82, RRID: AB_10854564) and confocal microscopy (D'Amario et al., 2011, 2014; Goichberg et al., 2013). The fraction of cells that reached replicative senescence and irreversible growth arrest was evaluated by the expression of the senescence-associated protein $p16^{INK4a}$ (Abcam: cat no. ab16123, RRID: AB_302274) (D'Amario et al., 2011, 2014; Goichberg et al., 2013). Apoptosis was measured in CPCs at baseline and following exposure to Doxo with the Annexin V detection assay (BD Pharmingen). Annexin V binds to the phosphatidylserine exposed on the outer leaflet of the cell membrane during apoptotic cell death. CPCs were seeded in 96 multi-well clear bottom black plates (3603, Corning); 24 h later, the medium was removed and cells were washed with PBS. FITC-Annexin V (556547, Pharmingen) diluted in binding buffer provided by the manufacturer was then added to the wells for a period of 30 min. After washing in PBS, cells were stained with DAPI. FITC (Excitation 490 nm; Emission 525 nm) and DAPI (Excitation 358 nm; Emission 461 nm) signals were quantified using Perkin Elmer EnVision Multilabel Reader. Apoptosis was calculated by normalizing the FITC signal to the number of cells represented by the DAPI signal.

2.10. DDR Foci and Comet Assay

CPCs were stained with a mouse *anti*-phospho-histone H2A.X (Ser139) (Millipore: cat. no. 05-636, RRID: AB_309864). Imaris software spot module was employed for the recognition of the γH2A.X-positive DDR foci and 3D rendering of the data (Goichberg et al., 2013). The number of foci per nucleus was counted utilizing the Imaris software.

The comet assay was performed utilizing the OxiSelect Comet Assay Kit (Cell Biolabs: cat. no. STA-351). Cells were embedded in agarose gel and placed on top of a microscope slide. Slides were treated with alkaline lysis buffer to remove proteins and, subsequently, immersed in TE buffer. Electrophoresis was performed to induce the formation of comets. Slides were stained with Vista green dye and analyzed by fluorescence microscopy (Lorenzo et al., 2013). The distance between the center of the head and the center of the tail, i.e. the tail moment length, was measured with ImageJ using comet assay plug-in. The tail moment was then calculated by the product of the percentage of damaged DNA and the tail moment length.

2.11. Western Blotting of CPCs

Protein lysates of CPCs were obtained using RIPA buffer (Sigma-Aldrich: cat. no. R0278) and protease inhibitors (Torella et al., 2004; Goichberg et al., 2013). Equivalents of 10 μg proteins were separated on 4–20% SDS-PAGE and subjected to traditional Western blotting. Additionally, equivalents of 1 μg proteins were analyzed with ProteinSimple Wes automated Western blotting system (Harris, 2015). The following antibodies were utilized: mouse monoclonal *anti*-p53 (Cell Signaling), rabbit polyclonal *anti*-p53 (Ser 37) (Cell Signaling Technology: cat. no. 2524, RRID: AB_331743), rabbit polyclonal *anti*-p53 (Ser15) (Cell Signaling Technology: cat. no. 9286S, RRID: AB_331741) and mouse monoclonal *anti*-$p16^{INK4a}$ (Cell Signaling Technology: cat. no. 8884S, RRID: AB_11129865). Loading conditions were determined by GAPDH.

2.12. qRT-PCR

Total RNA was extracted from CPCs with TRIzol Reagent (Invitrogen: cat. no. 15596018) and employed for the measurement of the quantity of transcripts of p53, Mdm2, Puma, Noxa, PIDD, Trp53inp, $p16^{INK4a}$, $p21^{Cip1}$, IGF-1 and PCNA. cDNA for mRNAs was obtained from 2 μg total RNA in a 20 μl reaction using High Capacity cDNA Reverse Transcription Kit (Applied Biosystems: cat. no. 4368814) and 100 pmole of oligo$(dT)_{15}$ primer (Hosoda et al., 2009; Goichberg et al., 2013). This mixture was incubated at 37 °C for 2 h. Quantitative RT-PCR was performed with primers designed using the Vector NTI (Invitrogen) software or downloaded from the NIH qdepot mouse primer database (for sequences see Supplementary Methods). StepOnePlus Real-Time PCR system (Applied Biosystems) was employed. cDNA synthesized from 100 ng total RNA was combined with Power SYBR Green PCR Master Mix (Applied Biosystems: cat. no. 4367659) and 0.5 μM each of forward and reverse primers. Cycling conditions were as follows: 95 °C for 10 min followed by 40 cycles of amplification (95 °C denaturation for 15 s, and 60 °C annealing-extension for 1 min). The melting curve was then obtained. To avoid the influence of genomic contamination, forward and reverse primers for each gene were located in different exons. Reactions with primers alone were also included as negative controls. Quantified values were normalized against the input determined by the housekeeping gene β2-microglobulin. Real-time PCR products were run on 2% agarose/1X TBE gel.

2.13. Diabetes and CPC Injection

C57Bl/6 female mice at 3–4 months of age were treated with streptozotocin (STZ, Sigma) for 7 consecutive days (~100 mg/kg body weight per day, i.p.) (Rota et al., 2006). STZ was dissolved in 0.9% saline solution containing 20 mM/l sodium citrate tribasic dehydrate (Sigma). Final STZ concentration was 5 mg/l. Animals developed hyperglycemia ~2 weeks after the last injection of STZ. TRUEtrack meter (Home Diagnostics, Inc.) and test strips were employed to measure blood glucose. Animals with blood glucose level > 400 mg/dl were included in the study.

Three–four weeks after the onset of hyperglycemia, 200,000 CPCs were injected within the myocardium (4 injections of 5 μl each). Mice were sacrificed 3 days following cell transplantation. Hearts were perfused with formalin and embedded in paraffin as described above. Tissue sections obtained from the mid-portion of the LV were stained for GFP (rabbit polyclonal *anti*-GFP, Molecular Probes: cat. no. A-11122, RRID: AB_221569; chicken polyclonal *anti*-GFP, Abcam: ab13970, RRID: AB_300798), α-sarcomeric actin (mouse *anti*-α-sarcomeric actin IgM, Sigma-Aldrich: cat. no. A2172, RRID: AB_476695), GATA4 (rabbit polyclonal *anti*-GATA4, Abcam: cat. no. ab84593, RRID: AB_10670538) and troponin I (mouse monoclonal *anti*-troponin I, Abcam: cat. no. ab10231, RRID: AB_296967). The number of GFP-positive cells per 10 mm^2 of myocardium was measured throughout the entire cross-section of the LV.

2.14. Data Analysis

Data are presented as mean ± SD. The Shapiro-Wilk test was utilized to define the normality of value distribution. In case of normal distribution, significance between two groups was determined by unpaired two-tailed Student's *t*-test. For multiple comparisons, the ANOVA test with the Bonferroni parametric correction was employed. When the normality test failed, the Mann-Whitney Rank Sum Test and the Kruskal-Wallis One Way ANOVA were employed. In all cases, $p < 0.05$ was considered significant (McDonald, 2014).

3. Results

3.1. p53 Does Not Alter the Mechanical and Growth Properties of Cardiomyocytes

The overexpression of p53 results in premature organism aging and animal mortality (Serrano and Blasco, 2007). The shorter lifespan may be due to defects in cardiac performance and myocyte mechanics, commonly found in the old failing heart (Leri et al., 2003; Torella et al., 2004; Signore et al., 2015). Therefore, we determined whether an increase in p53 gene dosage had a negative effect on ventricular hemodynamics and the electro-mechanical properties of cardiomyocytes. Wild-type (WT) and p53-tg mice at 3–6 and 24–31 months of age were studied. At both ages, left ventricular (LV) systolic pressure, LV end-diastolic pressure, LV developed pressure, and LV +dP/d*t* and −dP/d*t* did not differ in p53-tg and WT mice (Fig. 1a).

Moreover, Ca^{2+} transient amplitude, sarcomere shortening, and the timing parameters of Ca^{2+} transient and sarcomere shortening were measured in isolated LV myocytes. In all cases, no differences were found (Fig. 1b, c), suggesting that the physiological properties of the LV and cardiomyocytes were preserved in WT mice as a function of age, and a single extra gene-dose of p53 did not alter the function of the old heart. These observations are consistent with previous results in which aging effects have not been detected in WT 26 month-old C57BL/6J mice (Sanada et al., 2014).

To define further the characteristics of cardiomyocytes, the degree of cell replication and death was evaluated in young-adult, 8–11 months, and old, 20–25 months, WT and p53-tg mice. The fraction of cycling Ki67-positive myocytes and the percentage of apoptotic myocytes were similar in young WT and p53-tg and increased equally with age in both groups of mice (Fig. 2a, b). However, only the increase in cell

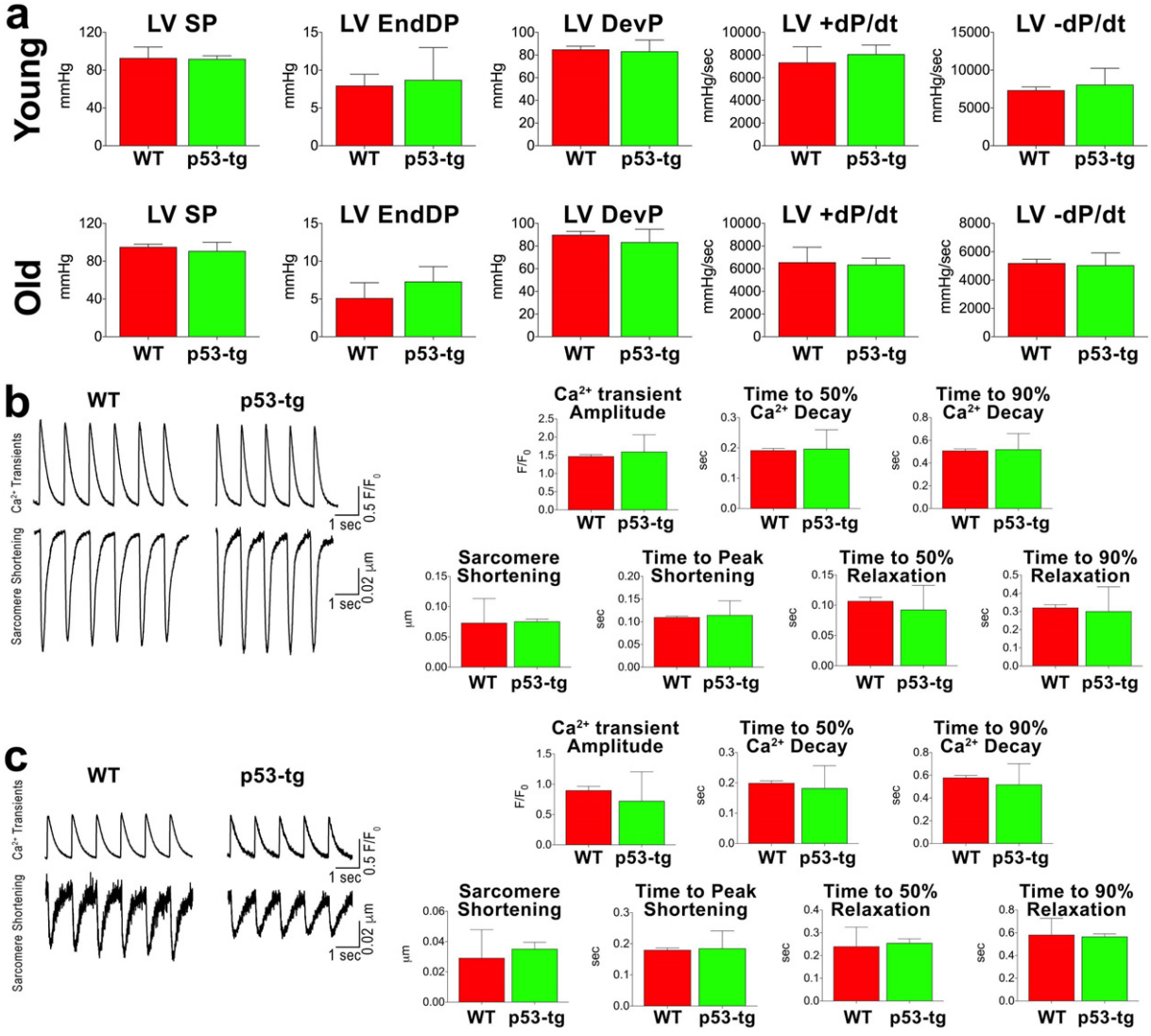

Fig. 1. Aging and p53 do not alter cardiac and myocyte function. (a) Hemodynamics in young-adult (3–6 months) and old (24–31 months) p53-tg and WT mice (young WT, $n = 9$, young p53-tg, $n = 7$; old WT, $n = 11$, old p53-tg, $n = 6$). LV SP, LV systolic pressure; LV EndDP, LV end-diastolic pressure; LV DevP, LV developed pressure. (b) Ca^{2+} transients and sarcomere shortening of cardiomyocytes in young WT ($n = 112$ cells from 10 mice) and young p53-tg ($n = 79$ cells from ±7 mice). (c) Ca^{2+} transients and sarcomere shortening of cardiomyocytes in old WT ($n = 40$ cells from 3 mice) and old p53-tg ($n = 25$ cells from 3 mice).

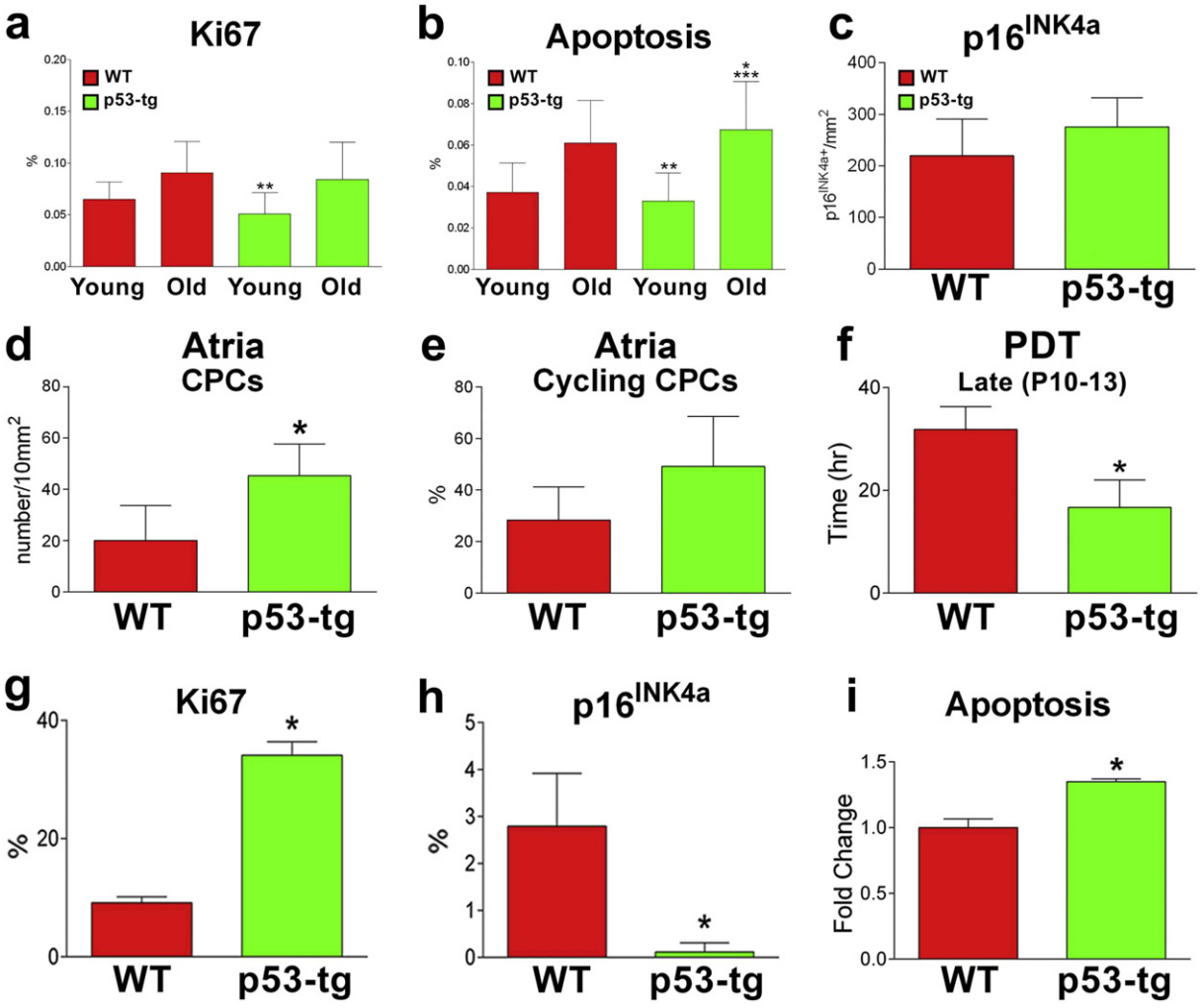

Fig. 2. p53, cardiomyocytes and CPCs. (a, b) Ki67-positive (a) and apoptotic TUNEL-positive (b) cardiomyocytes in young-adult, 8–11 months (WT: $n = 9$; p53-tg: $n = 7$), and old, 20–25 months (WT: $n = 6$; p53-tg: $n = 8$), WT and p53-tg mice. $^{*}p < 0.05$ vs. young-adult WT; $^{**}p < 0.05$ vs. old WT; $^{***}p < 0.05$ vs. young-adult p53-tg. (c) $p16^{INK4a}$-positive cardiomyocytes in old, 18–33 months, WT ($n = 4$) and p53-tg ($n = 9$) mice. (d, e) Number of *c*-kit-positive CPCs in atrial myocardium (d) and fraction of cycling Ki67-positive CPCs (e). WT: $n = 3$; p53-tg: $n = 4$. (f) Population doubling time (PDT) in WT-CPCs (WT; $n = 3$) and p53-tg-CPCs (p53-tg; $n = 3$). (g) Fraction of Ki67 labeled WT-CPCs ($n = 3$) and p53-tg-CPCs ($n = 3$). (h) Fraction of $p16^{INK4a}$ labeled WT-CPCs ($n = 3$) and p53-tg-CPCs ($n = 3$). (i) Apoptosis of WT-CPCs ($n = 3$) and p53-tg-CPCs ($n = 3$) measured by Annexin V assay. In all cases data are shown as mean ± SD. $^{*}p < 0.05$ vs. WT.

death in p53-tg hearts was statistically significant. Moreover, the number of senescent $p16^{INK4a}$-positive cardiomyocytes was comparable in 18–33 month-old WT and p53-tg (Fig. 2c), supporting the notion that the extra copy of p53 did not promote myocardial aging. This finding is typical of this model in which the p53 transgene is physiologically regulated and it is not constitutively active. Conversely, transgenic and mutant mice with chronically active p53 signaling are characterized by shortened lifespan (Matheu et al., 2008).

Cardiomyocyte apoptosis and aging are controlled in part by the expression of the p53-dependent genes, Bax and Bcl2, and the p53-regulated genes, angiotensinogen (Aogen) and angiotensin II (Ang II) type-1 receptors (AT1R) (Leri et al., 1998, 1999; Dimmeler and Leri, 2008; Xu et al., 2010). These parameters were measured in myocytes isolated from p53-tg and WT mice at 25 months of age. At the protein level, the quantity of the pro-apoptotic gene Bax and the anti-apoptotic gene Bcl2 was similar in WT and p53-tg myocytes (Fig. S1). Additionally, the levels of Aogen and AT1R did not differ in the two groups of cardiomyocytes (Fig. S1). Thus, an extra copy of p53 has no negative effects on cardiac performance, myocyte mechanics, Ca^{2+} transient, and cardiomyocyte growth, senescence and death.

3.2. p53 Preserves a Younger CPC Phenotype

CPC niches are preferentially located in the atrial myocardium (Sanada et al., 2014) so that a quantitative analysis was performed in this anatomical region of WT at 24–25 months and p53-tg at 24–31 months. The frequency of CPCs was significantly higher in p53-tg, while the fraction of replicating Ki67-positive CPCs was similar in the two groups (Fig. 2d, e). Because of these two variables, a larger pool of cycling CPCs was present in the atria of p53-tg mice.

To evaluate the growth reserve of CPCs, these cells were isolated from the myocardium of p53-tg at 26–30 months and WT at 23–25 months; cells were expanded in vitro and population doubling time (PDT) was determined at P10-P13. PDT was 47% shorter in p53-tg-CPCs than in WT-CPCs (Fig. 2f). Moreover, the percentage of Ki67-positive CPCs at P10-P13 was 3.9-fold higher in p53-tg-CPCs (1528/4561; 33.5%) than in WT-CPCs (543/6235; 8.7%) (Fig. 2g). At later passages, P16-P17, $p16^{INK4a}$ comprised 2.9% of WT-CPCs (36/1255; 2.9%) and only 0.03% of p53-tg-CPCs (1/3275; 0.03%) (Fig. 2h). However, apoptosis was 35% higher in p53-tg-CPCs (Fig. 2i), despite the lower number of senescent cells. Thus, an extra copy of the p53 allele preserves a

younger CPC phenotype after propagation in vitro and prevents the accumulation of senescent CPCs by potentiating cell death.

3.3. p53 Increases the Repair of DNA Damage in CPCs

Reactive oxygen species (ROS) induce foci of injury in the telomeric and non-telomeric DNA; this affects the growth and viability of the target cells (Schieber and Chandel, 2014). To evaluate whether p53-tg-CPCs had a superior, equal or inferior ability to sustain ROS-mediated DNA damage than WT-CPCs, these stem cell classes were exposed to a low dose of doxorubicin (Doxo) which is coupled with the formation of DNA strand breaks (Goichberg et al., 2013).

The γH2A.X protein accumulates at regions of DNA strand breaks, allowing the recognition of DNA damage (Mohrin et al., 2010; Goichberg et al., 2013). The localization of γH2A.X increased from 4.7% (200/4284; 4.7%) to 29% (1148/3958; 29%) in WT-CPCs and from 2.2% (296/13334; 2.2%) to 73.8% (12,185/16496; 73.8%) in p53-tg-CPCs (Fig. 3a, b). These results suggest that p53-tg-CPCs were 2.5-fold more

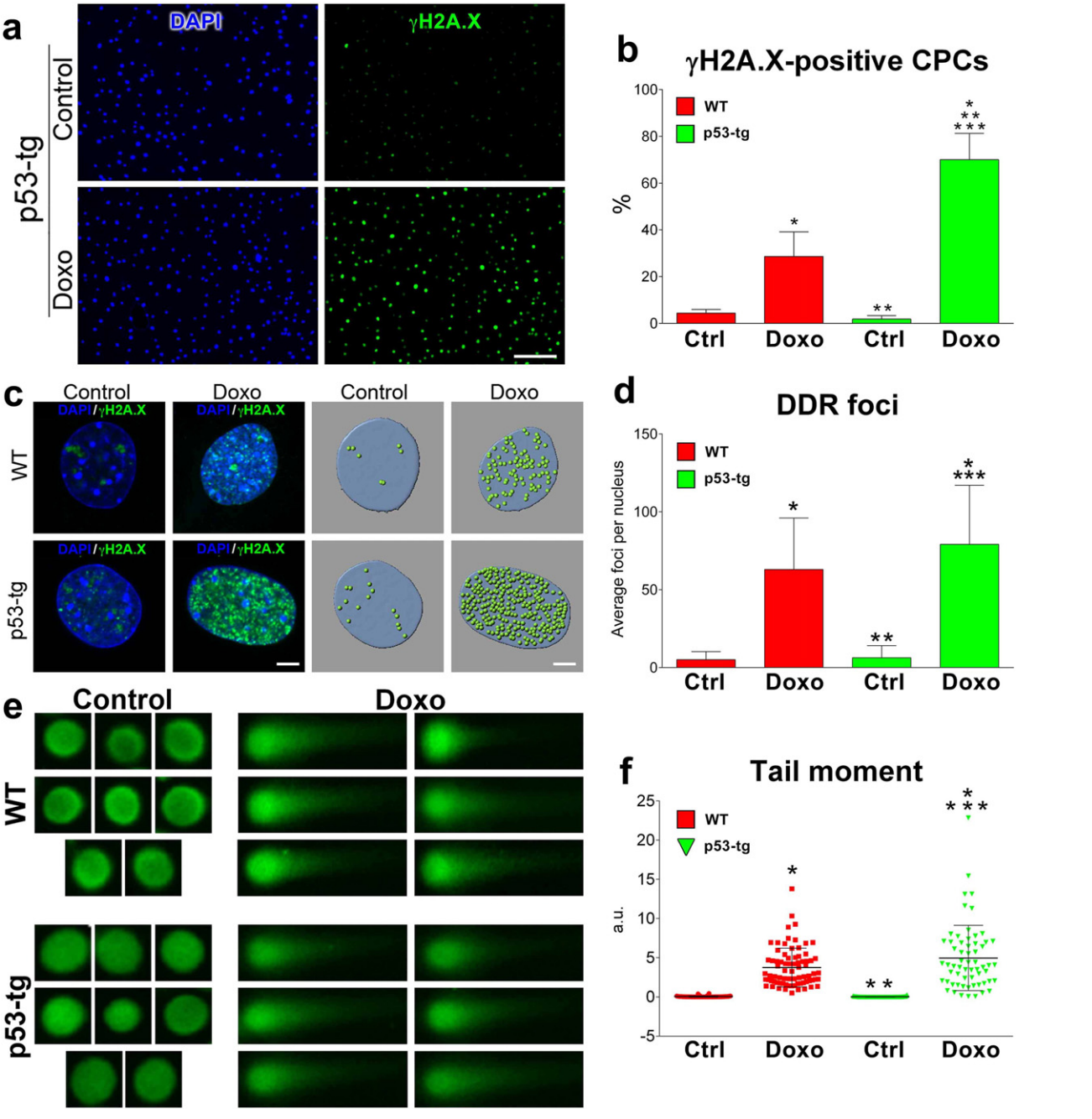

Fig. 3. p53 improves the DDR of CPCs. (a) Nuclei from p53-tg-CPCs in the absence (Control) and in the presence of Doxo are stained by DAPI (blue, left panels); immunolabeled γH2A.X is shown in these nuclei (green, right panels). Scale bar: 100 μm. (b) Fraction of γH2A.X-positive CPCs in the absence (control, Ctrl) and following exposure to Doxo (Doxo): Ctrl WT-CPCs (4284 cells from 3 mice); Ctrl p53-tg-CPCs (13,334 cells from 3 mice); Doxo WT-CPCs (3958 cells from 3 mice); and Doxo p53-tg-CPCs (16,496 cells from 3 mice). Data are mean ± SD. (c) γH2A.X (green; left two panels) in nuclei of WT-CPCs and p53-tg-CPCs stained by DAPI (blue). DDR foci are illustrated in the same nuclei following three-dimensional reconstruction by Imaris version 5.5.2 (right two panels). Scale bar: 5 μm. (d) Number of DDR foci counted in nuclei of WT-CPCs and p53-tg-CPCs. In each case, 24–59 γH2A.X positive nuclei from 3 mice were analyzed. (e) Nucleoids of WT-CPCs and p53-tg-CPCs are stained with Vista green dye (green, left panels). Comets are apparent after Doxo (green, right panels). (f) Quantity of damaged DNA in nuclei of WT-CPCs and p53-tg-CPCs at baseline (Control: WT, $n = 62$ comets from 3 mice; p53-tg, $n = 70$ comets from 3 mice) and after Doxo (Doxo: WT, $n = 76$ comets from 3 mice; p53-tg, $n = 61$ comets from 3 mice). $^{*}p < 0.05$ vs. WT Ctrl; $^{**}p < 0.05$ vs. Doxo WT-CPCs; $^{***}p < 0.05$ vs. p53-tg Ctrl.

efficient than WT-CPCs in recruiting γH2A.X at the sites of DNA damage, a process necessary for the initiation of DNA repair (Fumagalli et al., 2012). However, the enhanced recruitment of γH2A.X at the sites of DNA damage in p53-tg-CPCs may be independent from the extra copy of the p53 allele; p53-tg-CPCs possess a younger cell phenotype (see Fig. 2h, i), which may determine the higher efficiency of DNA repair in this progenitor cell class.

DDR foci correspond to the localization of the γH2A.X protein at the level of DNA lesions. In the presence of Doxo, the incidence of DDR foci per nucleus (p53-tgCPCs, baseline: 6.3; WT-CPCs, baseline: 5.1; p53-tgCPCs, Doxo: 79; WT-CPCs, Doxo: 63) increased markedly and in a similar manner, 12-fold, in p53-tg-CPCs and WT-CPCs (Fig. 3c, d), although a larger fraction of p53-tg-CPCs recruited γH2A.X, as shown in Fig. 3b. High values of DDR foci per nucleus may indicate an effective completion of DNA repair and/or a more extensive DNA damage (Lukas et al., 2011). To test this possibility the degree of DNA damage in the two categories of CPCs was determined by the Comet assay (Lorenzo et al., 2013).

CPCs were embedded in agarose on microscope slides and lysed to form nucleoids. Electrophoresis was performed to identify structures resembling comets at fluorescence microscopy (Fig. 3e). The fluorescence intensity of the tail (damaged DNA) relative to the head (intact DNA) reflects the percentage of DNA damage; 61–76 comets were analyzed in WT-CPCs and p53-tg-CPCs in the absence and presence of Doxo. The distance between the center of the head and the center of the tail, i.e. the tail moment length, indicates the frequency of DNA strand breaks. The tail moment was calculated by the product of the percentage of damaged DNA and the tail moment length. The tail moment provides a parameter that comprises both the extent of DNA damage and the frequency of DNA strand breaks; this index was found to be comparable at baseline and to increase similarly in p53-tg-CPCs and WT-CPCs following Doxo (Fig. 3f). Thus, the extent of damaged DNA promoted by oxidative stress was analogous in the two CPC classes (see Fig. 3d), but a larger fraction of cells carrying an extra copy of the p53 allele recruited γH2A.X (see Fig. 3b), possibly enhancing DNA repair.

3.4. p53 Enhances the Expression of Genes Regulating DDR

The tumor suppressor p53 trans-activates several genes implicated in the cell cycle and apoptosis (Riley et al., 2008), and an increase in p53 gene dosage may impact on the function of CPCs. Therefore, the expression of p53 and its target genes was measured in p53-tg-CPCs and WT-CPCs in the absence and presence of Doxo. At baseline, the quantity of p53 was similar in the two stem cell categories (Fig. 4a–c). After 4 h of Doxo, p53 levels increased and p53 phosphorylation at Ser-18, a post-translational modification required for p53 DNA binding, was present in both WT-CPCs and p53-tg-CPCs. At baseline, p53 phosphorylation at Ser-34 was high in WT-CPCs and in p53-tg-CPCs and with Doxo decreased in both stem cell categories (Fig. 4b, c). Together with other sites of post-translational modifications, phosphorylation of p53 at Ser-34 is relevant to DDR (Loughery and Meek, 2013).

The expression of p53 and other genes (Riley et al., 2008) implicated in inhibition of p53 activity (Mdm2), induction of apoptosis (Puma and Noxa), protection from oxidative stress (Trp53inp), cellular senescence ($p16^{INK4a}$), cell cycle arrest and DNA repair ($p21^{Cip1}$), and proliferation (IGF-1 and PCNA), was measured by qRT-PCR. The expression of PIDD was also determined; PIDD is a master regulator of cell fate decision, playing a critical role in DNA repair, cell proliferation, survival and death (Bock et al., 2012).

At baseline, p53, PIDD, IGF-1 and PCNA transcripts were higher and $p21^{Cip1}$ was lower in p53-tg-CPCs than in WT-CPCs, possibly reflecting the enhanced proliferative activity of cells with an extra copy of the p53 gene (Fig. 4d). With Doxo treatment, Mdm2, Puma and $p21^{Cip1}$ increased mostly in p53-tg-CPCs, suggesting that $p21^{Cip1}$ promoted cell cycle arrest and favored DNA repair. However, $p16^{INK4a}$ was decreased in p53-tg-CPCs. PIDD and Trp53inp were upregulated in p53-tg-CPCs and WT-CPCs, but the changes in Trp53inp were greater in p53-tg-CPCs; thus, the protection from oxidative stress was enhanced in p53-tg-CPCs (Fig. 4d). With Doxo, the expression of IGF-1 and PCNA decreased in p53-tg-CPCs and these changes are consistent with activation of the DNA repair process. In WT-CPCs, Doxo led to an attenuation of IGF-1 and an upregulation of Noxa, which may mediate cell apoptosis.

The temporal changes in the expression of p53, Mdm2, $p21^{Cip1}$, Noxa, PIDD, Trp53inp and Puma were evaluated in p53-tg-CPCs and WT-CPCs from time 0 to 120 min following Doxo-treatment (Fig. S2). In p53-tg-CPCs, the expression of p53 appeared to increase earlier than the upregulation of Mdm2, $p21^{Cip1}$, PIDD, Trp53inp and Puma. These adaptations suggest that oxidative stress was coupled with a rapid response in the genes modulating p53 function, growth arrest, oxidative DNA damage and repair, and cell death. Conversely, in WT-CPCs, the modest increase in p53 was associated with a time-dependent increase in the pro-apoptotic gene Noxa (Fig. S2).

The expression of Noxa and Puma is essential for p53-mediated apoptosis; in this regard, the deletion of these two genes prevents cell death in response to stimuli leading to upregulation of p53 activity (Valente et al., 2013). The differential expression of Noxa and Puma in WT-CPCs and p53-tg-CPCs with oxidative stress may depend on the distinct post-translational modifications of p53, which condition the transactivation of specific target genes. Additionally, γH2A.X, which is more effectively recruited at the sites of DNA damage in p53-tg-CPCs, promotes upregulation of Puma independently from p53 signaling (Xu et al., 2016). Thus, p53 is a critical determinant of stem cell fate and an extra copy of the p53 allele positively impacts on the survival and growth of CPCs.

3.5. p53 Promotes DNA Repair and Recovery of CPC Growth

To determine whether the distinct response of CPC classes to oxidative stress was translated in a differential recovery in function, p53-tg-CPCs and WT-CPCs were exposed to Doxo for 4 h (Doxo-pulse) and, after Doxo removal, cellular senescence, DNA repair and proliferation were measured following a 72-hour recovery period (Recovery). After recovery, $p16^{INK4a}$ expression was barely detectable by Western blotting in p53-tg-CPCs, but was upregulated in WT-CPCs (Fig. 5a). Similarly, by immunolabeling and confocal microscopy, a small fraction of $p16^{INK4a}$-positive cells was identified in p53-tg-CPCs, while numerous WT-CPCs expressed $p16^{INK4a}$ [Fig. 5b; (WT-CPCs: control = 6/610, 0.98%; Doxo pulse = 22/1742, 1.26%; Recovery = 150/2877, 5.2%) (p53-tg-CPCs: control = 6/1903, 0.3.2%; Doxo pulse = 3/4293, 0.07%; Recovery = 32/3473, 0.9%)]. Importantly, following recovery, the number of DDR foci and the tail moment decreased dramatically in p53-tg-CPCs; however, these parameters remained high in WT-CPCs (Fig. 5c–e). Additionally, a progressive increase in cell proliferation was observed in p53-tg-CPCs from 24 to 48 and 72 h after the removal of Doxo [Fig. 5f; (WT-CPCs: 24 h = 143/8167, 1.7%; 48 h = 511/8405, 6.1%; 72 h = 270/4915, 5.4%) (p53-tg-CPCs: 24 h = 305/7902, 0.3.9%; 48 h = 1443/13635, 11%; 72 h = 1032/6246, 17%)]. In contrast, the reinstitution of cell proliferation was modest in WT-CPCs. Thus, following oxidative stress, an extra copy of the p53 allele potentiates the ability of CPCs to reestablish the integrity of the DNA, leading to a relevant restoration of cell growth.

3.6. p53 Increases the Engraftment of CPCs in the Diabetic Heart

The in vitro results discussed thus far have suggested that p53-tg-CPCs have the capacity to grow extensively in vitro and are more resistant to ROS than WT-CPCs. These two characteristics are critical for the successful implementation of cell therapy for the pathologic heart. Tissue reconstitution involves isolation, in vitro expansion and delivery of CPCs to the damaged myocardium, where the hostile environment and high levels of oxidative stress (Kizil et al., 2015) interfere with the cardiac repair process and cardiomyocyte regeneration (Broughton

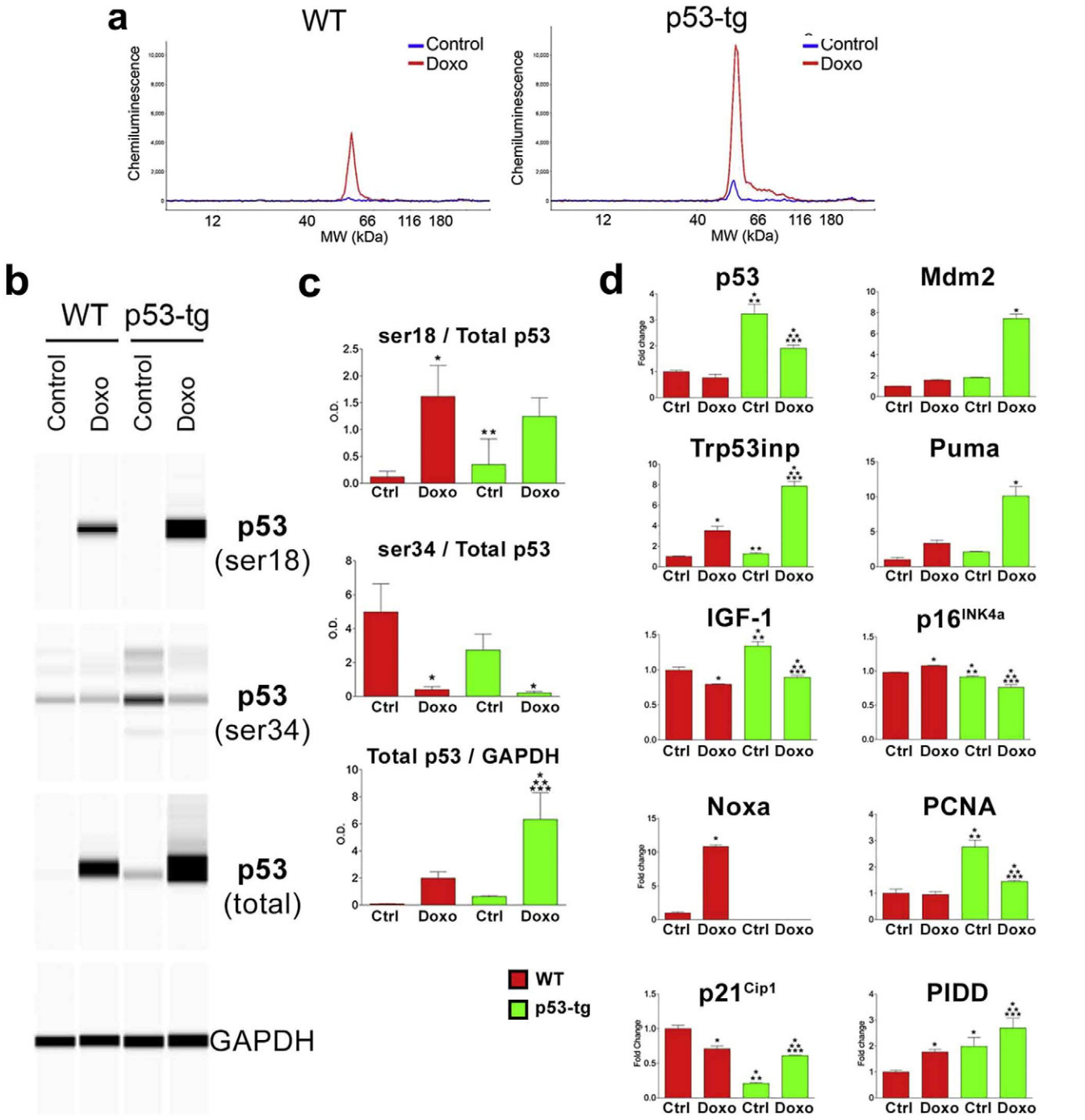

Fig. 4. p53 and p53-dependent genes. (a) Quantity of p53 protein by automated Wes Western blotting in WT-CPCs (WT) and p53-tg-CPCs (p53-tg) at baseline (blue line) and after Doxo (red line). Tracings illustrate the peak level of p53 in the four CPC classes; $n = 3$ in all cases. (b) The pseudo-blots show the expression of phosphorylated p53 at Ser-18 and Ser-34, and p53 and GAPDH in the four CPC classes. (c) Quantitative data are shown as mean ± SD. $^{*}p < 0.05$ vs. WT Ctrl. $^{**}p < 0.05$ vs. WT Doxo. $^{***}p < 0.05$ vs. p53-tg Ctrl. (d) mRNA level of p53 and p53 regulated genes in the CPC classes at baseline (Ctrl) and after Doxo; $n = 3$ in all cases. Ct values above 35 cycles were considered not detectable. For statistics see panel B.

and Sussman, 2016). To test whether p53-tg-CPCs retained in vivo the properties documented in vitro, both WT-CPCs and p53-tg-CPCs were injected intramyocardially in diabetic mice 3–4 weeks after the administration of streptozotocin when the blood glucose level was >400 mg/dl. This model was selected because is characterized by enhanced oxygen toxicity (Rota et al., 2006). Animals, 4 in each group, were sacrificed 3 days later when engraftment of CPCs is expected to be completed and cell differentiation may begin to occur. This protocol was based on previous observations concerning the engraftment and lineage specification of *c*-kit-positive hematopoietic stem cells delivered to the damaged myocardium (Rota et al., 2007). Four injections of EGFP-labeled CPCs were performed in different sites of the LV wall. Diabetes was characterized by foci of tissue injury where both WT-CPCs and p53-tg-CPCs homed (Fig. 6; Fig. S3) and began to acquire the cardiomyocyte phenotype (Fig. 7a–d). Quantitatively, the number of EGFP-positive cells in the LV myocardium was 2350/10 mm^2 and 1590/10 mm^2 in diabetic mice treated with p53-tg-CPCs and WT-CPCs, respectively (Fig. 7e).

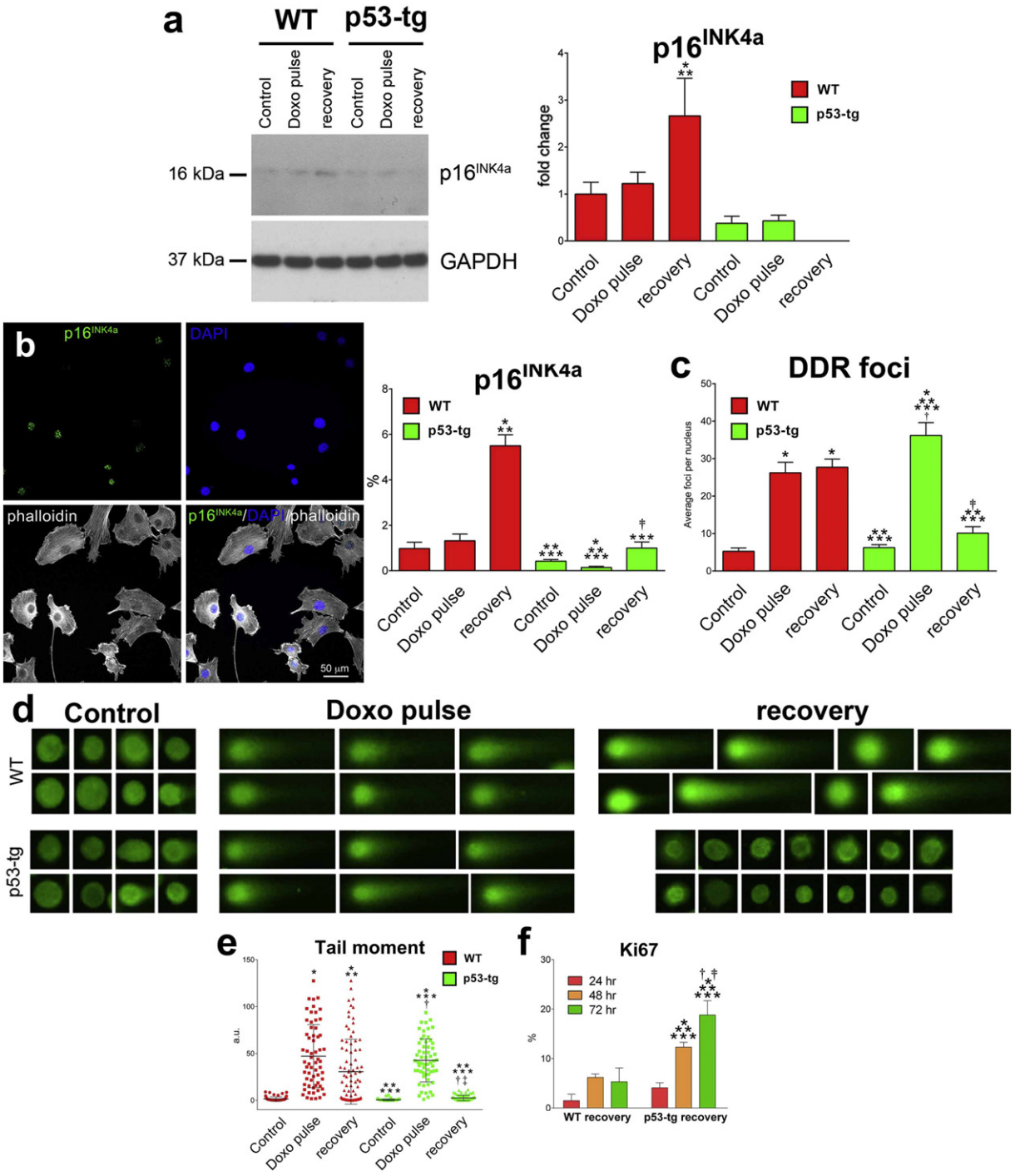

Fig. 5. p53 favors the functional recovery of CPCs from oxidative stress in vitro. (a) Western blotting of $p16^{INK4a}$ at baseline, after Doxo-pulse and following recovery of WT-CPCs (WT) and p53-tg-CPCs (p53-tg); $n = 3$ in all cases. Optical density data are mean ± SD. $^{*}p < 0.05$ vs. WT-Control. $^{**}p < 0.05$ vs. WT-Doxo-pulse. $^{***}p < 0.05$ vs. WT-recovery. (b) $p16^{INK4a}$ labeling (upper left panel, yellow) of WT-CPCs exposed to Doxo. Nuclei are stained by DAPI (upper right panel, blue). Phalloidin (lower left panel, white). Merge of $p16^{INK4a}$, DAPI and phalloidin (lower right panel). Scale bar, 50 μm. Fraction of $p16^{INK4a}$-positive WT-CPCs and p53-tg-CPCs at baseline, following Doxo-pulse and after recovery; $n = 3$ in all cases. Data are mean ± SD. $^{*}p < 0.05$ vs. WT-Control. $^{**}p < 0.05$ vs. WT-Doxo-pulse. $^{***}p < 0.05$ vs. WT recovery. $^{\dagger}p < 0.05$ vs. p53-tg control. $^{\ddagger}p < 0.05$ vs. p53-tg Doxo-pulse. (c) Number of DDR foci in WT-CPCs and p53-tg-CPCs at baseline, after Doxo-pulse and following recovery; $n = 3$ in all cases. For statistics see panel B. (d) Nucleoids in WT-CPCs and p53-tg-CPCs at baseline, following Doxo-pulse and after recovery are stained with Vista green dye (green). Comets are apparent in Doxo-pulse and after recovery of WT-CPCs, while intact DNA is noted in p53-tg-CPCs after recovery. (e) Damaged DNA in nuclei of WT-CPCs and p53-tg-CPCs at baseline, after Doxo-pulse and following recovery; $n = 3$ in all cases. For statistics see panel B. (f) Fraction of Ki67-positive WT-CPCs and p53-tg-CPCs following 24, 48 and 72 h recovery period; $n = 3$ in all cases.$^{*}p < 0.05$ vs. 24 h. $^{**}p < 0.05$ vs. 48 h.

Additionally, clusters of EGFP-positive cells in the early stage of myocyte commitment were recognized by the expression of the transcription factor GATA4 (Fig. 8; Fig. S4). The volume of these developing myocytes can be expected to increase with time and reach in part an adult cell phenotype, as observed previously by in situ activation of endogenous CPCs after myocardial infarction. Importantly, the generation of parenchymal cells in that setting was associated with growth of both resistance arterioles and capillary profiles (Urbanek et al., 2005). Thus,

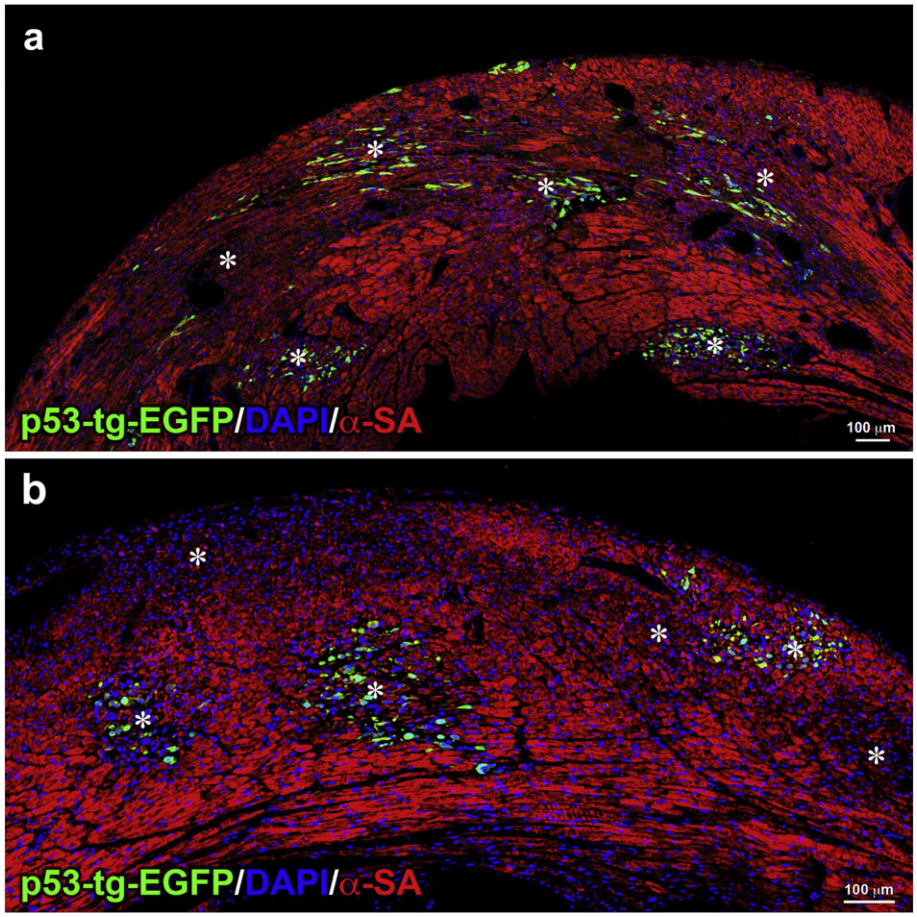

Fig. 6. p53-tg-CPCs engraft in the diabetic heart. (a, b) Areas of myocardial damage (*) in the LV wall; EGFP-positive (green) p53-tg-CPCs are engrafted in the majority of these foci of injury. Cardiomyocytes are labeled by α-sarcomeric actin (α-SA; red).

CPCs carrying an extra copy of the p53 gene have an intrinsic advantage and a superior cellular regenerative response after injection in the diabetic heart.

4. Discussion

The results of the current study indicate that CPCs obtained from the heart of old mice carrying an extra gene-dose of p53 can be propagated extensively in vitro retaining an impressive growth reserve at late passages. Based on this genetic modification, large quantities of CPCs can be generated, raising the possibility that multiple temporally distinct deliveries of cells can be introduced to restore the structural and functional integrity of the damaged myocardium. This critical aspect of autologous cell therapy has recently been documented experimentally (Tokita et al., 2016). Although it might be intuitively obvious that one injection of CPCs cannot reverse cardiac pathology, this work has provided the information needed for the development of a better strategy for the treatment of human heart failure. Thus, a large number of the patient's own CPCs is required, together with the ability of the expanded cells to engraft within the unfavorable environment of the diseased heart.

As documented in the current study, the enhanced expression of p53 leads to a complex cellular response which involves a network of genes implicated in DNA repair and cell proliferation, and cellular senescence and apoptosis (Fig. S5). The extra copy of the p53 gene improves the ability of CPCs to sustain oxidative stress, an adaptation mediated by a rapid restoration of the integrity of the DNA and cell division. The prompt and efficient recruitment of DDR proteins at the sites of DNA strand breaks in p53-tg-CPCs reflects the mechanism needed to counteract the consequences of DNA damaging agents, typically present in the diabetic, old and failing heart (Frustaci et al., 2000; Dimmeler and Leri, 2008; Goichberg et al., 2014). Conversely, CPCs with unmodified quantity of endogenous p53 are less resistant to oxidative stress and fail to mend proficiently DNA strand breaks, a defect that results in irreversible growth arrest and cell death. Thus, p53-tg-CPCs have a significant biological and therapeutic advantage with respect to WT-CPCs; they manifest a higher survival rate when delivered in vivo enhancing cell homing and potentially myocardial regeneration. The increased dosage of p53 provides CPCs with critical defense mechanisms necessary for the cells to remain viable in the adverse milieu of the diabetic and failing heart.

Despite severe hyperglycemia and its toxic consequences, p53-tg-CPCs engraft more effectively than WT-CPCs within the sites of damage present throughout the myocardium of diabetic mice and initiate a reparative process. The difference in the magnitude of cell homing observed with WT-CPCs and p53-tg-CPCs in the presence of diabetes underscores how critical is the function of p53 in enhancing the ability of the delivered cells to colonize the injured ventricle, a condition necessary for the successful replacement of cardiomyocytes lost as a result of cardiac pathology (Leri et al., 2015).

Human CPCs have recently been introduced in the management of heart failure in patients suffering from post-infarction ischemic cardiomyopathy with encouraging results (Chugh et al., 2012; Makkar et al., 2012). However, several clinical trials with a variety of progenitor cells have been performed in the last decade in similar patient cohorts but the outcome has been inconsistent (Afzal et al., 2015). Despite the use of large number of cells, there is general agreement that the fraction of engrafted cells is miniscule and this limitation precludes an efficient recovery of the injured myocardium. The strategy employed here may

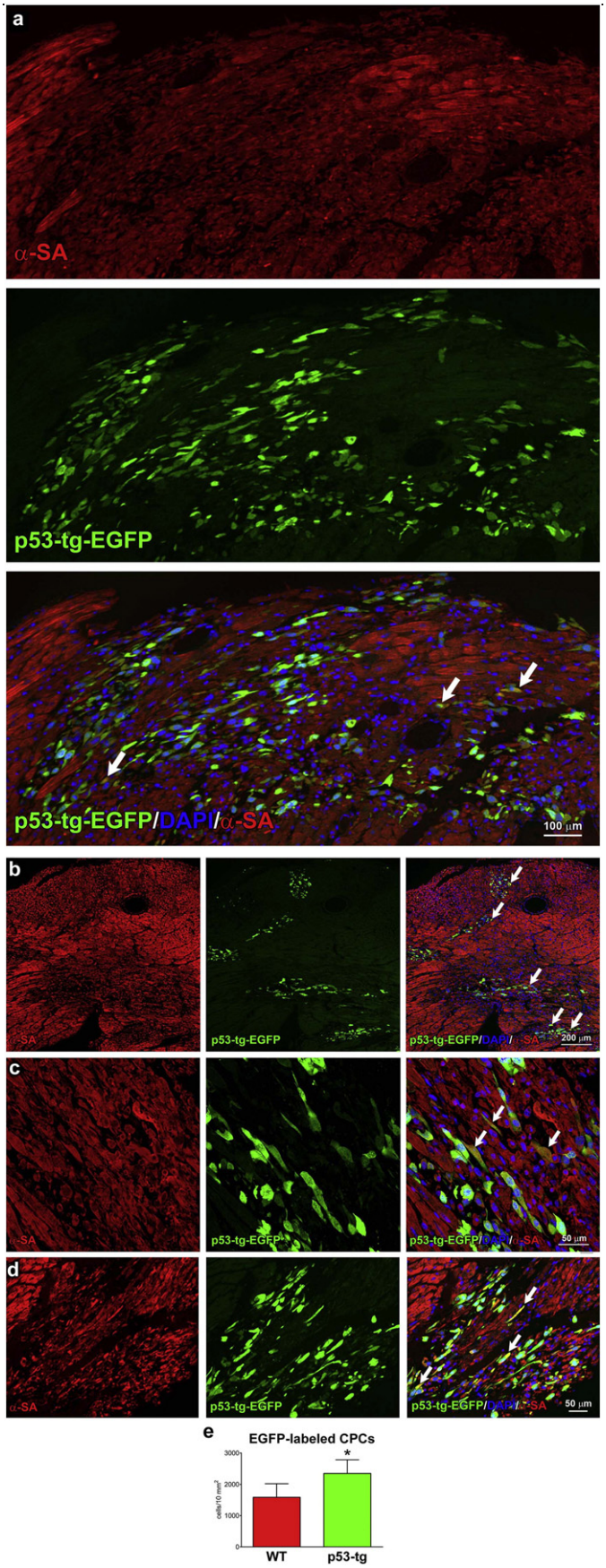

overcome in part this problem and make stem cell therapy more effective in restoring the structural and functional integrity of the decompensated human heart.

Poor survival and limited retention of adoptively transferred stem cells in the pathologic heart may reduce significantly the efficacy of regenerative therapy. Stem cell viability is influenced by the ischemic condition and inflammatory response of the recipient myocardium and the intrinsic properties of donor cells (Broughton and Sussman, 2016). Several strategies have been utilized to reduce the susceptibility of the delivered cells to die and prolong the window of time available for their engraftment within the damaged myocardium. Preconditioning of CPCs with a variety of cytokines potentiates their resistance to oxidative stress, favoring their migration and recruitment.

A more prolonged effect is obtained when stem cells are genetically modified to express anti-apoptotic mediators. Canonical regulators of myocyte survival, oncogenic proteins and factors involved in the development of embryonic-fetal myocyte progenitors have been employed (Broughton and Sussman, 2016). The serine/threonine Pim-1 kinase which is a downstream target of Akt favors the engraftment and lineage commitment of CPCs and long-term myocardial regeneration (Cottage et al., 2012; Mohsin et al., 2013). CPCs obtained by p53-tg mice show characteristics similar to those observed in the presence of Pim-1: the increased proliferation and delayed cell aging in vitro are accompanied by enhanced engraftment and survival in vivo. The extra gene copy of p53, however, provides an additional advantage through the selective depletion of old damaged stem cells maintaining a pool of progenitors with a younger cell phenotype.

The structural integration of the delivered CPCs with the recipient organ is the primary event that conditions the long-term recovery of the lost myocardium. However, in the current study, we did not evaluate the durability of the process, which will be determined in future work with the expectation that the injected p53-tg-CPCs will differentiate and generate mature, functionally-competent cardiomyocytes, together with the required coronary microcirculation. At the early time point, the injected WT-CPCs and p53-tg-CPCs were restricted to the injured regions of the ventricular wall. The microenvironment of the damaged diabetic myocardium is unquestionably hostile although obligatory for cell homing. The transplantation of progenitor cells in the intact tissue results in cell apoptosis (Tillmanns et al., 2008).

The function of p53 as fate modulator has been studied in several stem cell systems, where it exerts opposite functions, which appear to be context and cell type dependent. p53 orchestrates the polarity of self-renewing divisions in neural stem cells and coordinates the timing for cell fate specification (Quadrato and Di Giovanni, 2012). During steady-state hematopoiesis, the basal-level of p53 activity regulates the quiescence and self-renewal of hematopoietic stem cells (HSCs) expanding the immature cell pool (Liu et al., 2009a). This phenomenon may overcome the decline in HSC function observed with aging, although a larger pool of HSCs with intense self-renewal capacity may favor the development of leukemia (Asai et al., 2011).

The ability of the heart to maintain the steady state and respond to injury declines with aging and diabetes (Eming et al., 2014). The composition of the stem cell pool changes in both cases, favoring the accumulation of cells that do not self-renew and may manifest a skewed pattern of lineage choices. Apoptosis is restricted to $p16^{INK4a}$-positive CPCs, but the process of clearance of old CPCs is inefficient resulting in their progressive accumulation (Sanada et al., 2014). Enhanced p53 expression corrects the abnormal behavior of CPCs, modifying their fate. As shown here, in the presence of oxidative stress, p53 upregulates the

Fig. 7. p53 expands the engraftment of CPCs within the diabetic myocardium. (a–d) Areas of myocardial regeneration shown at different magnification contain small developing cardiomyocytes, which express EGFP and α-SA (yellow; arrows). (e) Number of EGFP-positive cells per 10 mm^2 of myocardium in diabetic hearts injected with WT-CPCs ($n = 4$) or p53-tg-CPCs ($n = 4$). Data are mean ± SD. $^*p < 0.05$ vs. WT-CPCs.

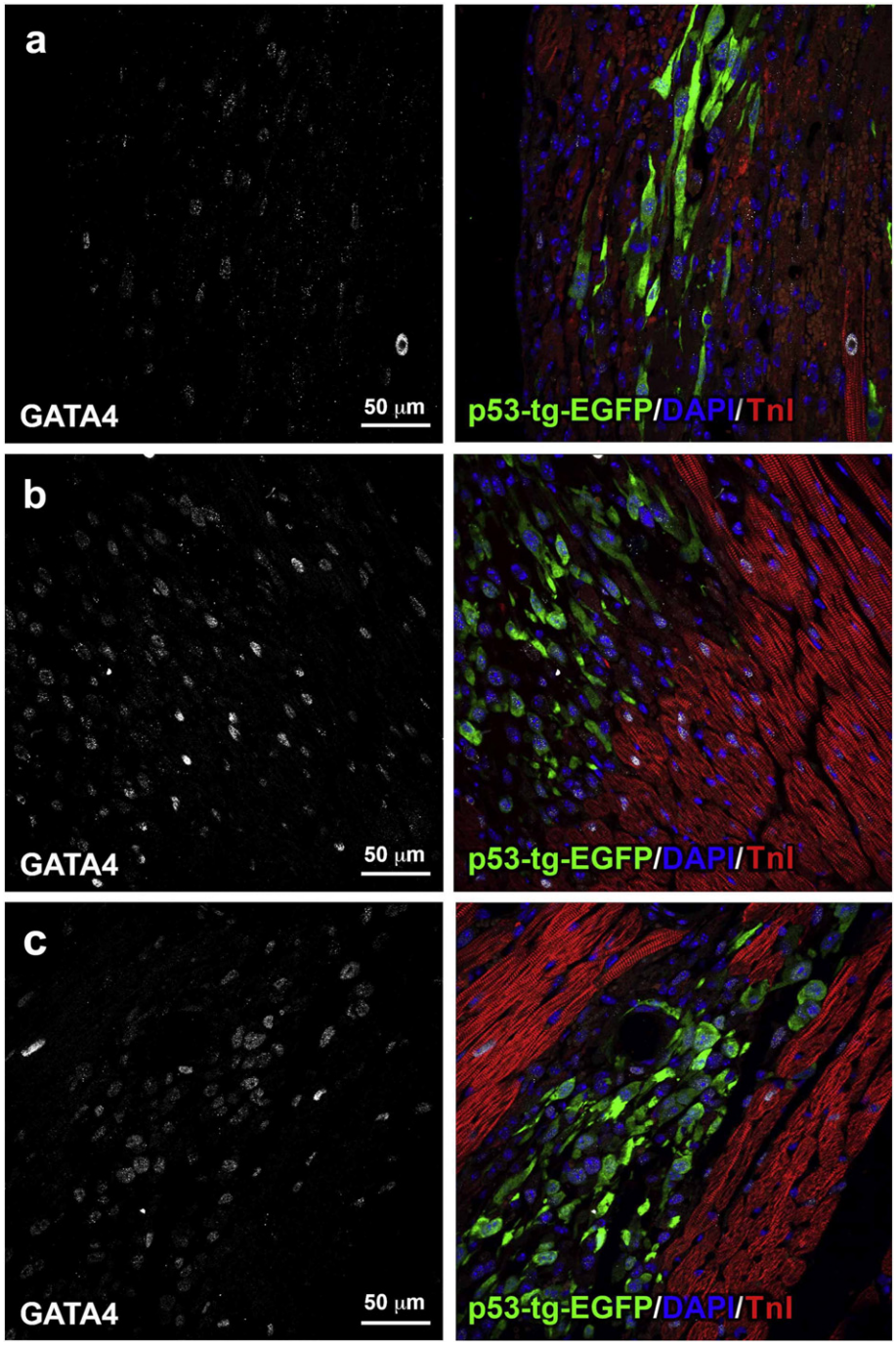

Fig. 8. Early commitment of p53-tg-CPCs. (a-c) GATA4 is expressed (left, white) in EGFP-positive cells (right, green) distributed within the damaged diabetic myocardium. Cardiomyocytes are labeled by troponin I (right, TnI: red).

expression of Trp53inp and PIDD in CPCs ameliorating DDR. Additionally, p53 increases the level of Puma favoring apoptosis of damaged CPCs. Thus, p53, through cell death activation, prevents the secretory activity of senescent CPCs which release a variety of molecules exerting pro-aging effects on the surrounding young cells (Tchkonia et al., 2013).

Stem cells constitute a long-lived replicative cell population that experiences prolonged periods of quiescence. Stem cell quiescence protects from endogenous stresses mediated by cell respiration and DNA division, but these functions are attenuated by oxidative stress. Old, rarely dividing cells show more γH2AX foci than actively proliferating cells (Rossi et al., 2007; Liu et al., 2009b), since the molecular control of DNA repair is intimately linked to the progression of the cell cycle. Importantly, the extent of DNA damage is comparable in WT-CPCs and p53-tg-CPCs but the enhanced expression of p53 expands the pool of cells displaying DDR foci. This biological response supports the view that CPCs genetically modified to express physiologically regulated p53 are protected from environmental stimuli and genomic lesions. DNA repair maintains genomic integrity and attenuates the rate of aging of p53-tg-CPCs.

Whether the enhanced expression of p53 improves the intrinsic properties of CPCs, or the intact resident stem cell compartment is activated by the intramyocardial injection of specific growth factors, these cells are responsible for myocyte and coronary vessel regeneration (Beltrami et al., 2003; Sanada et al., 2014; Liu et al., 2015). The replicative reserve of *c*-kit-positive CPCs predicts the evolution of ischemic cardiomyopathy following revascularization in humans (D'Amario et al.,

2014) and profound defects in human CPC function are present with advanced heart failure (Urbanek et al., 2003, 2005) and in the decompensated senescent human heart (Chimenti et al., 2003). CPCs are the critical determinant of human cardiac pathology and strategies increasing their growth and reparative process may have important clinical implications.

These experimental results cannot be translated to human beings without caveats. Mouse CPCs differ from human CPCs. The latter are isolated from small samples of diseased myocardium although intact CPCs with maintained growth reserve have always been found (D'Amario et al., 2011).

Supplementary data to this article can be found online at http://dx.doi.org/10.1016/j.ebiom.2017.01.028.

Funding Sources

This work was supported by grants from the National Institutes of Health (NIH) (P01-AG023071) and by Cardiocentro Ticino Foundation (R01AG37490). Our funding sources played no role in how the research was conducted.

Conflict of Interest

P.A. is a member of Autologous LLC and AAL Scientifics Inc. A.L. is a member of AAL Scientifics Inc. The other authors did not report any conflict of interest.

Author Contributions

R.K. and A.M. designed and conducted the experiments, analyzed the data and participated in the writing of the manuscript; J.F-M., E.Z., G.P., A.C., M. C. C-D-S., A. B-C., F.S., N.I. prepared reagents and conducted the experiments; M.R. prepared reagents and conducted experiments and analyzed part the data; M.A.B., M.S., participated in the discussion of the study and critically reviewed the manuscript; P.A. analyzed the data and participated in the writing of the manuscript; A.L. designed the experiments, analyzed the data and wrote the manuscript.

All co-authors reviewed critically the manuscript and gave final approval of the manuscript to be submitted.

Acknowledgments

None.

References

Afzal, M.R., Samanta, A., Shah, Z.I., Jeevanantham, V., Abdel-Latif, A., Zuba-Surma, E.K., Dawn, B., 2015. Adult bone marrow cell therapy for ischemic heart disease: evidence and insights from randomized controlled trials. Circ. Res. 117, 558–575.

Asai, T., Liu, Y., Bae, N., Nimer, S.D., 2011. The p53 tumor suppressor protein regulates hematopoietic stem cell fate. J. Cell. Physiol. 226, 2215–2221.

Beausejour, C.M., Campisi, J., 2006. Ageing: balancing regeneration and cancer. Nature 443, 404–405.

Beltrami, A.P., Barlucchi, L., Torella, D., Baker, M., Limana, F., Chimenti, S., Kasahara, H., Rota, M., Musso, E., Urbanek, K., et al., 2003. Adult cardiac stem cells are multipotent and support myocardial regeneration. Cell 114, 763–776.

Bock, F.J., Peintner, L., Tanzer, M., Manzl, C., Villunger, A., 2012. P53-induced protein with a death domain (PIDD): master of puppets? Oncogene 31, 4733–4739.

Broughton, K.M., Sussman, M.A., 2016. Empowering adult stem cells for myocardial regeneration v2.0: success in small steps. Circ. Res. 118, 867–880.

Cheng, Z., Ito, S., Nishio, N., Thanasegaran, S., Fang, H., Isobe, K., 2013. Characteristics of cardiac aging in C57BL/6 mice. Exp. Gerontol. 48, 341–348.

Chimenti, C., Kajstura, J., Torella, D., Urbanek, K., Heleniak, H., Colussi, C., Di Meglio, F., Nadal-Ginard, B., Frustaci, A., Leri, A., et al., 2003. Senescence and death of primitive cells and myocytes lead to premature cardiac aging and heart failure. Circ. Res. 93, 604–613.

Chugh, A.R., Beache, G.M., Loughran, J.H., Mewton, N., Elmore, J.B., Kajstura, J., Pappas, P., Tatooles, A., Stoddard, M.F., Lima, J.A., et al., 2012. Administration of cardiac stem cells in patients with ischemic cardiomyopathy: the SCIPIO trial: surgical aspects and interim analysis of myocardial function and viability by magnetic resonance. Circulation 126, S54–S64.

Cottage, C.T., Neidig, L., Sundararaman, B., Din, S., Joyo, A.Y., Bailey, B., Gude, N., Hariharan, N., Sussman, M.A., 2012. Increased mitotic rate coincident with transient telomere lengthening resulting from pim-1 overexpression in cardiac progenitor cells. Stem Cells 30, 2512–2522.

D'Amario, D., Fiorini, C., Campbell, P.M., Goichberg, P., Sanada, F., Zheng, H., Hosoda, T., Rota, M., Connell, J.M., et al., 2011. Functionally competent cardiac stem cells can be isolated from endomyocardial biopsies of patients with advanced cardiomyopathies. Circ. Res. 108, 857–861.

D'Amario, D., Leone, A.M., Iaconelli, A., Luciani, M., Gaudino, M., Kannappan, R., Manchi, M., Severino, A., Shin, S.H., Graziani, F., et al., 2014. Growth properties of cardiac stem cells are a novel biomarker of patients' outcome after coronary bypass surgery. Circulation 129, 157–172.

Dimmeler, S., Leri, A., 2008. Aging and disease as modifiers of efficacy of cell therapy. Circ. Res. 102, 1319–1330.

Eming, S.A., Martin, P., Tomic-Canic, M., 2014. Wound repair and regeneration: mechanisms, signaling, and translation. Sci. Transl. Med. 6 (265sr6).

Frustaci, A., Kajstura, J., Chimenti, C., Jakoniuk, I., Leri, A., Maseri, A., Nadal-Ginard, B., Anversa, P., 2000. Myocardial cell death in human diabetes. Circ. Res. 87, 1123–1132.

Fumagalli, M., Rossiello, F., Clerici, M., Barozzi, S., Cittaro, D., Kaplunov, J.M., Bucci, G., Dobreva, M., Matti, V., Beausejour, C.M., et al., 2012. Telomeric DNA damage is irreparable and causes persistent DNA-damage-response activation. Nat. Cell Biol. 14, 355–365.

Garcia-Cao, I., Garcia-Cao, M., Martin-Caballero, J., Criado, L.M., Klatt, P., Flores, J.M., Weill, J.C., Blasco, M.A., Serrano, M., 2002. "Super p53" mice exhibit enhanced DNA damage response, are tumor resistant and age normally. EMBO J. 21, 6225–6235.

Garcia-Cao, I., Garcia-Cao, M., Tomas-Loba, A., Martin-Caballero, J., Flores, J.M., Klatt, P., Blasco, M.A., Serrano, M., 2006. Increased p53 activity does not accelerate telomere-driven ageing. EMBO Rep. 7, 546–552.

Goichberg, P., Kannappan, R., Cimini, M., Bai, Y., Sanada, F., Sorrentino, A., Signore, S., Kajstura, J., Rota, M., Anversa, P., et al., 2013. Age-associated defects in EphA2 signaling impair the migration of human cardiac progenitor cells. Circulation 128, 2211–2223.

Goichberg, P., Chang, J., Liao, R., Leri, A., 2014. Cardiac stem cells: biology and clinical applications. Antioxid. Redox Signal. 21, 2002–2017.

Hachamovitch, R., Wicker, P., Capasso, J.M., Anversa, P., 1989. Alterations of coronary blood flow and reserve with aging in Fischer 344 rats. Am. J. Phys. 256, H66–H73.

Harris, V.M., 2015. Protein detection by simple Western analysis. Methods Mol. Biol. 1312, 465–468.

Hosoda, T., D'Amario, D., Cabral-Da-Silva, M.C., Zheng, H., Padin-Iruegas, M.E., Ogorek, B., Ferreira-Martins, J., Yasuzawa-Amano, S., Amano, K., Ide-Iwata, N., 2009. Clonality of mouse and human cardiomyogenesis in vivo. Proc. Natl. Acad. Sci. U. S. A. 106, 17169–17174.

Kizil, C., Kyritsis, N., Brand, M., 2015. Effects of inflammation on stem cells: together they strive? EMBO Rep. 16, 416–426.

Leri, A., Claudio, P.P., Li, Q., Wang, X., Reiss, K., Wang, S., Malhotra, A., Kajstura, J., Anversa, P., 1998. Stretch-mediated release of angiotensin II induces myocyte apoptosis by activating p53 that enhances the local renin-angiotensin system and decreases the Bcl-2-to-Bax protein ratio in the cell. J. Clin. Invest. 101, 1326–1342.

Leri, A., Liu, Y., Wang, X., Kajstura, J., Malhotra, A., Meggs, L.G., Anversa, P., 1999. Overexpression of insulin-like growth factor-1 attenuates the myocyte renin-angiotensin system in transgenic mice. Circ. Res. 84, 752–762.

Leri, A., Franco, S., Zacheo, A., Barlucchi, L., Chimenti, S., Limana, F., Nadal-Ginard, B., Kajstura, J., Anversa, P., Blasco, M.A., 2003. Ablation of telomerase and telomere loss leads to cardiac dilatation and heart failure associated with p53 upregulation. EMBO J. 22, 131–139.

Leri, A., Rota, M., Pasqualini, F.S., Goichberg, P., Anversa, P., 2015. Origin of cardiomyocytes in the adult heart. Circ. Res. 116, 150–166.

Liu, Y., Elf, S.E., Miyata, Y., Sashida, G., Liu, Y., Huang, G., Di Giandomenico, S., Lee, J.M., Deblasio, A., Menendez, S., et al., 2009a. p53 regulates hematopoietic stem cell quiescence. Cell Stem Cell 4, 37–48.

Liu, Y., Elf, S.E., Asai, T., Miyata, Y., Liu, Y., Sashida, G., Huang, G., Di Giandomenico, S., Koff, A., Nimer, S.D., 2009b. The p53 tumor suppressor protein is a critical regulator of hematopoietic stem cell behavior. Cell Cycle 8, 3120–3124.

Liu, X., Hall, S.R., Wang, Z., Huang, H., Ghanta, S., Di Sante, M., Leri, A., Anversa, P., Perrella, M., 2015. Rescue of neonatal cardiac dysfunction in mice by administration of cardiac progenitor cells in utero. Nat. Commun. 6, 8825.

Lorenzo, Y., Costa, S., Collins, A.R., Azqueta, A., 2013. The comet assay, DNA damage, DNA repair and cytotoxicity: hedgehogs are not always dead. Mutagenesis 28, 427–432.

Loughery, J., Meek, D., 2013. Switching on p53: an essential role for protein phosphorylation? BioDiscovery 8, 1.

Lukas, J., Lukas, C., Bartek, J., 2011. More than just a focus: the chromatin response to DNA damage and its role in genome integrity maintenance. Nat. Cell Biol. 13, 1161–1169.

Makkar, R.R., Smith, R.R., Cheng, K., Malliaras, K., Thomson, L.E., Berman, D., Czer, L.S., Marban, L., Mendizabal, A., Johnston, P.V., et al., 2012. Intracoronary cardiosphere-derived cells for heart regeneration after myocardial infarction (CADUCEUS): a prospective, randomised phase 1 trial. Lancet 379, 895–904.

Matheu, A., Maraver, A., Klatt, P., Flores, I., Garcia-Cao, I., Borras, C., Flores, J.M., Viña, J., Blasco, M.A., Serrano, M., 2007. Delayed ageing through damage protection by the Arf/p53 pathway. Nature 448, 375–379.

Matheu, A., Maraver, A., Serrano, M., 2008. The Arf/p53 pathway in cancer and aging. Cancer Res. 68, 6031–6034.

McDonald, J.H., 2014. Handbook of Biological Statistics. third ed. Sparky House Publishing, Baltimore, Maryland.

Mohrin, M., Bourke, E., Alexander, D., Warr, M.R., Barry-Holson, K., Le Beau, M.M., Morrison, C.G., Passegue, E., 2010. Hematopoietic stem cell quiescence promotes error-prone DNA repair and mutagenesis. Cell Stem Cell 7, 174–185.

Mohsin, S., Khan, M., Nguyen, J., Alkatib, M., Siddiqi, S., Hariharan, N., Wallach, K., Monsanto, M., Gude, N., Dembitsky, W., et al., 2013. Rejuvenation of human cardiac progenitor cells with Pim-1 kinase. Circ. Res. 113, 1169–1179.

Quadrato, G., Di Giovanni, S., 2012. Gatekeeper between quiescence and differentiation: p53 in axonal outgrowth and neurogenesis. Int. Rev. Neurobiol. 105, 71–89.

Riley, T., Sontag, E., Chen, P., Levine, A., 2008. Transcriptional control of human p53-regulated genes. Nat. Rev. Mol. Cell. Biol. 9, 402–412.

Rossi, D.J., Seita, J., Czechowicz, A., Bhattacharya, D., Bryder, D., Weissman, I.L., 2007. Hematopoietic stem cell quiescence attenuates DNA damage response and permits DNA damage accumulation during aging. Cell Cycle 6, 2371–2376.

Rota, M., LeCapitaine, N., Hosoda, T., Boni, A., De Angelis, A., Padin-Iruegas, M.E., Esposito, G., Vitale, S., Urbanek, K., Casarsa, C., et al., 2006. Diabetes promotes cardiac stem cell aging and heart failure, which are prevented by deletion of the p66shc gene. Circ. Res. 99, 42–52.

Rota, M., Kajstura, J., Hosoda, T., Bearzi, C., Vitale, S., Esposito, G., Iaffaldano, G., Padin-Iruegas, M.E., Gonzalez, A., Rizzi, R., et al., 2007. Bone marrow cells adopt the cardiomyogenic fate in vivo. Proc. Natl. Acad. Sci. U. S. A. 104, 17783–17788.

Sanada, F., Kim, J., Czarna, A., Chan, N.Y., Signore, S., Ogorek, B., Isobe, K., Wybieralska, E., Borghetti, G., Pesapane, A., et al., 2014. c-kit-positive cardiac stem cells nested in hypoxic niches are activated by stem cell factor reversing the aging myopathy. Circ. Res. 114, 41–55.

Schieber, M., Chandel, N.S., 2014. ROS function in redox signaling and oxidative stress. Curr. Biol. 24, R453–R462.

Serrano, M., Blasco, M.A., 2007. Cancer and ageing: convergent and divergent mechanisms. Nat. Rev. Mol. Cell. Biol. 8, 715–722.

Signore, S., Sorrentino, A., Borghetti, G., Cannata, A., Meo, M., Zhou, Y., Kannappan, R., Pasqualini, F., O'Malley, H., Sundman, M., et al., 2015. Late Na (+) current and protracted electrical recovery are critical determinants of the aging myopathy. Nat. Commun. 6, 8803.

Tchkonia, T., Zhu, Y., van Deursen, J., Campisi, J., Kirkland, J.L., 2013. Cellular senescence and the senescent secretory phenotype: therapeutic opportunities. J. Clin. Invest. 123, 966–972.

Tillmanns, J., Rota, M., Hosoda, T., Misao, Y., Esposito, G., Gonzalez, A., Vitale, S., Parolin, C., Yasuzawa-Amano, S., Muraski, J., et al., 2008. Formation of large coronary arteries by cardiac progenitor cells. Proc. Natl. Acad. Sci. U. S. A. 105, 1668–1673.

Tokita, Y., Tang, X.L., Li, Q., Wysoczynski, M., Hong, K.U., Nakamura, S., Wu, W.J., Xie, W., Li, D., Hunt, G., et al., 2016. Repeated administrations of cardiac progenitor cells are markedly more effective than a single administration: a new paradigm in cell therapy. Circ. Res. 119, 635–651.

Torella, D., Rota, M., Nurzynska, D., Musso, E., Monsen, A., Shiraishi, I., Zias, E., Walsh, K., Rosenzweig, A., Sussman, M.A., et al., 2004. Cardiac stem cell and myocyte aging, heart failure, and insulin-like growth factor-1 overexpression. Circ. Res. 94, 514–524.

Urbanek, K., Quaini, F., Tasca, G., Torella, D., Castaldo, C., Nadal-Ginard, B., Leri, A., Kajstura, J., Quaini, E., Anversa, P., 2003. Intense myocyte formation from cardiac stem cells in human cardiac hypertrophy. Proc. Natl. Acad. Sci. U. S. A. 100, 10440–10445.

Urbanek, K., Torella, D., Sheikh, F., De Angelis, A., Nurzynska, D., Silvestri, F., Beltrami, C.A., Bussani, R., Beltrami, A.P., Quaini, F., et al., 2005. Myocardial regeneration by activation of multipotent cardiac stem cells in ischemic heart failure. Proc. Natl. Acad. Sci. U. S. A. 102, 8692–8697.

Valente, L.J., Gray, D.H., Michalak, E.M., Pinon-Hofbauer, J., Egle, A., Scott, C.L., Janic, A., Strasser, A., 2013. p53 efficiently suppresses tumor development in the complete absence of its cell-cycle inhibitory and proapoptotic effectors p21, Puma, and Noxa. Cell Rep. 3, 1339–1345.

Xu, J., Carretero, O.A., Liao, T.D., Peng, H., Shesely, E.G., Xu, J., Liu, T.S., Yang, J.J., Reudelhuber, T.L., Yang, X.P., 2010. Local angiotensin II aggravates cardiac remodeling in hypertension. Am. J. Physiol. Heart Circ. Physiol. 299, H1328–H1338.

Xu, C., Zhang, L., Duan, L., Lu, C., 2016. MicroRNA-3196 is inhibited by H2AX phosphorylation and attenuates lung cancer cell apoptosis by downregulating PUMA. Oncotarget 7, 77764–77776.